Astronomy & Astrophysics manuscript no. a383_oiii
December 5, 2025

Highly-ionized gas in lensed $z = 6.027$ Little Red Dot seen through [O III] 88μm with ALMA

Kirsten K. Knudsen[1⋆], Johan Richard[2], Mathilde Jauzac[3,4,5,6], Tom J.L.C. Bakx[1], Thiago S. Gonçalves[7], Eiichi Egami[8], Kiana Kade[1], Rahul Rana[1], Laura Sommovigo[9,10] Flora Stanley[11], and Daniel P. Stark[8]

[1] Department of Space, Earth and Environment, Chalmers University of Technology, SE-412 96 Gothenburg, Sweden
[2] CRAL, Observatoire de Lyon, Université Lyon 1, 9 Avenue Ch. André, F-69561 Saint Genis Laval Cedex, France
[3] Centre for Extragalactic Astronomy, Durham University, South Road, Durham DH1 3LE, U.K.
[4] Institute for Computational Cosmology, Durham University, South Road, Durham DH1 3LE, U.K.
[5] Astrophysics Research Centre, University of KwaZulu-Natal, Westville Campus, Durban 4041, South Africa
[6] School of Mathematics, Statistics & Computer Science, University of KwaZulu-Natal, Westville Campus, Durban 4041, South Africa
[7] Observatório do Valongo, Universidade Federal do Rio de Janeiro, Ladeira do Pedro Antônio 43, Saúde, Rio de Janeiro, RJ 20080-090, Brazil
[8] Steward Observatory, University of Arizona, 933 N Cherry Ave, Tucson, AZ 85721, USA
[9] Department of Astronomy, Columbia University, 550 W 120th St, New York, NY 10025, USA
[10] Center for Computational Astrophysics, Flatiron Institute, 162 5th Avenue, New York, NY 10010, USA
[11] Institut de Radioastronomie Millimétrique (IRAM), 300 Rue de la Piscine, F-38400 Saint-Martin-d'Hères, France

Received ... / Accepted ...

ABSTRACT

Determining the physical properties of galaxies during the first billion years after the big bang is key to understanding both early galaxy evolution and how galaxies contributed to the epoch of reionization. We present deep ALMA observations of the redshifted [O III] 88 μm line for the gravitationally lensed (μ = 11.4 ± 1.9) galaxy A383-5.1 (z = 6.027) that has previously been detected in [C II] 158 μm. Recent *James Webb Space Telescope* (*JWST*) imaging identified this sub-L* galaxy as a "Little Red Dot" (LRD). With a line luminosity of $L_{[\rm OIII]} = (1.29 \pm 0.24) \times 10^8$ L$_\odot$ (corrected for lensing magnification) A383-5.1 is one of the faintest galaxies with combined [C II] and [O III] detections. The ALMA data reveal no dust continuum emission, consistent with previous observations. The high line luminosity ratio of [O III]/ [C II] ~ 14 ± 5 is consistent with A383-5.1 being low-metallicity and dust-poor. The non-detection of dust continuum in bands 6 and 8 is consistent with the high [O III]/[C II] ratio and suggests a presence of a strong ultraviolet radiation field, which would be less affect by dust attenuation, implying that galaxies of this type could contribute significantly to the ionization of the intergalactic medium. The presence of strong ionizing field could provide an important piece of information for understanding the nature of LRDs and their role in cosmic reionization.

Key words. Galaxies: high-redshift – Galaxies: evolution – Galaxies: ISM – Galaxies: individual: A383-5.1 – Submillimeter: galaxies

1. Introduction

The first billion years after the big bang mark the rise in galaxy formation and galaxy evolution, which is witnessed for example by the increased integrated star formation rate (e.g., summarised in reviews, Madau & Dickinson 2014; Stark 2016). The ultraviolet (UV) emission produced in galaxies ionize the neutral hydrogen of the integalactic medium, marking the phase transition from neutral to ionized medium at cosmological scales, also known as the epoch of reionization (EoR). The end of the EoR is estimated to be around redshift $z \sim 6$ (e.g., Stark 2016; Planck Collaboration et al. 2016). It has long been debated whether the dominant sources of ionizing UV-photons are the bright, but rarer quasars and active galactic nuclei (AGN), or the less luminous, but more common, normal to low-luminosity galaxies (e.g. Fontanot et al. 2012; Grissom et al. 2014; Hassan et al. 2018). Observations of the luminosity function at $z > 5$ show an increased significance of the faint-end compared to the bright-end, supporting the claim that the dominant fraction of UV-photons could arise from the common low-luminosity galaxies (e.g. McLure et al. 2013; Bouwens et al. 2016; Parsa et al. 2018).

Determining the physical properties of galaxies during and at the end of the EoR provides necessary constraints for understanding the nature of the sources that could be responsible for the bulk of the UV-emission giving rise to the re-ionisation. This also provides insights for characterising the early galaxy evolution. With the increasing number of galaxies with spectroscopic redshift at $z > 6$ (e.g. Schenker et al. 2012; Shibuya et al. 2012; Finkelstein et al. 2013; Oesch et al. 2015; Zitrin et al. 2015), it is possible to study the physical properties using, for example, the far-infrared fine-structure lines [C II] and [O III] (e.g. Ouchi et al. 2013; Ota et al. 2014; Maiolino et al. 2015; Knudsen et al. 2016; Inoue et al. 2016; Bradač et al. 2017; Laporte et al. 2017; Hashimoto et al. 2018; Fujimoto et al. 2021; Jolly et al. 2021; Bouwens et al. 2022; Fudamoto et al. 2022; Algera et al. 2024a; Fujimoto et al. 2024) and search for dust emission (e.g. Watson et al. 2015; Laporte et al. 2017, 2021; Sommovigo et al. 2022; Inami et al. 2022).

⋆ E-mail: kirsten.knudsen@chalmers.se

The ionization potential of neutral oxygen is similar to that of hydrogen, and the ionization potential of ionized oxygen is 35 eV. Double ionization of oxygen requires a UV-radiation field characteristic of O-type stars and that of AGN. As a result, doubly ionized oxygen is typically found in H II regions. Double ionized oxygen has two far-infrared fine-structure lines at 52 μm and 88 μm. The latter is observed to be very bright in star-forming galaxies, at a line intensity similar to that of the [C II] 158 μm line (e.g. De Looze et al. 2014), and in the low-metallicity dwarf galaxies it is seen to be brighter than the [C II] line (e.g. Cormier et al. 2015). This makes it a very attractive line to study in $z > 6$ galaxies, as it is also redshifted to submm wavelengths, and [O III] 88 μm is detected in a small number $z > 7$ galaxies (e.g. Inoue et al. 2016; Laporte et al. 2017; Hashimoto et al. 2018; Harikane et al. 2020).

In this paper we present Atacama Large Millimetre/Submillimetre Array (ALMA) observations of [O III] 88μm in the sub-L^*, gravitationally lensed galaxy A383-5.1 (z = 6.027). With the combination of the extensive ALMA integration time invested to this project and the gravitational lensing magnification, which is estimated to be $\mu = 11.4 \pm 1.9$ (Richard et al. 2011; Stark et al. 2015), this is among the deepest observations for a single high-z source carried out with ALMA. Based on an analysis of the optical and near-infrared spectroscopy and photometry of the counter-image A383-5.2, the system has an estimated SFR of $2.0^{+0.34}_{-0.3}$ $M_\odot$ yr^{-1}, a stellar mass of $M_{\rm stellar} = (3.2^{+0.8}_{-0.7})\times10^9$ $M_\odot$, and a very bright Lyα line, which could imply a somewhat higher SFR (Richard et al. 2011; Stark et al. 2015). Furthermore, the modelling from Stark et al. (2015) shows that the galaxy is best described by a two-component star formation history, where a young starburst component contributes only little to the stellar mass, but contributes significantly to the ionizing radiation. Also, the counter-image A383-5.2 has a near-infrared spectroscopic detection of C III], and A383-5.1 has one of the lowest-luminosity [C II] detections published so-far (Richard et al. 2011; Stark et al. 2015; Knudsen et al. 2016).

New *James Webb Space Telescope (JWST)*/NIRCam observations reveal that rest-frame optical images of A383-5.1 and 5.2 consists of two components, namely a 'Little Red Dot' (LRD) and a blue component (Golubchik et al. 2025; Baggen et al. 2025). LRDs are an extremely red population of sources found in *JWST* observations (e.g., Kocevski et al. 2023; Labbé et al. 2023, 2025). These galaxies exhibit unusual properties including distinctive V-shaped spectral slopes, broad emission lines, generally lacking X-ray emission, and no dust and radio detections (e.g., Kocevski et al. 2023; Labbé et al. 2023, 2025; Greene et al. 2024; Casey et al. 2025; Maiolino et al. 2025; Perger et al. 2025). Providing a clear explanation for these properties has been challenging. A leading explanation is the 'Black Hole *' (BH*) model wherein the AGN at the center of the LRD is surrounded by a dense screen of hydrogen (Naidu et al. 2025). The SED of one component of the A383-5.1 system exhibits the V-shape characteristic of LRDs (Golubchik et al. 2025; Baggen et al. 2025), although it should be noted that the LRD classification is tentative until spectroscopic confirmation can be carried out. Golubchik et al. (2025) found that the SED of the LRD component was best fit by a BH* model whereas the blue component was found to be most consistent with a young star-forming nebular object. Golubchik et al. (2025) suggested that a possible explanation of this system is that the blue object is metal-enriched emission that was ejected from the red component hosting the LRD. Baggen et al. (2025) suggested that the blue component is a young star-forming population, while the red component could be fit with a massive and dusty source. However, they also discuss that the red component could be interpreted as a combination of stellar and AGN emission. The detection of [C II] and [O III] in A383-5.1 are the first detections of far-infrared emission lines in an LRD. The ALMA data presented here provide additional input to the discussion on the nature of A383-5.1.

We assume a ΛCDM cosmology with $H_0 = 67.4\,{\rm km\,s^{-1}\,Mpc^{-1}}$, $\Omega_M = 0.315$, and $\Omega_\Lambda = 0.685$ (Planck Collaboration et al. 2020).

2. Observations

We have obtained ALMA observations of the redshifted [O III] 3393.00624 GHz line in A383-5.1 (project ID 2016.1.00333.S). The observations were carried out using the band-8 receiver during cycle-4 and 5 (Sekimoto et al. 2008). Ten executions were done resulting in a total on-source integration time of 8 hours. For the receivers one spectral window was tuned to redshifted [O III] line based on the redshift derived from the [C II] detection (Knudsen et al. 2016) with a bandwidth of 1.875 GHz and spectral resolution of 3.906 MHz (using Frequency Division Mode). The three other available spectral windows used a continuum setup with a bandwidth of 2 GHz each distributed over 128 channels (using Time Division Mode). The telescope configuration has baselines extending between 15 and 783 m.

The Common Astronomy Software Application (CASA McMullin et al. 2007) was used for reduction, calibration, and imaging. The pipeline reduced data delivered by the observatory was of sufficient quality, therefore no additional flagging and further calibration were done. The ALMA pipeline includes the steps required for standard reduction and calibration, such as flagging, bandpass calibration, as well as flux and gain calibrations. A conservative estimate of the absolute flux calibration is 10%, based on the ALMA Technical Handbook (Remijan et al. 2019).

Imaging both the continuum and spectral cube using natural weighting the resulting resolution is $0.37'' \times 0.32''$ PA = -84° and the r.m.s. is 35 μJy beam^{-1} and 0.41 mJy beam^{-1} (in a $\sim$ 20 km s^{-1} channel), respectively.

Moreover, we extract additional [C II] data from the ALMA archive from project 2015.1.01136.S, which had 60% of the observing time compared to our old [C II] data, but does add twice as long baselines. Data were reduced following standard procedures, and then combined with our previous data, resulting in an angular resolution of $0.33'' \times 0.29''$ PA = -80° and an rms of 0.17 mJy beam^{-1} (in a $\sim$ 17 km s^{-1} channel).

3. Results

We detect the redshifted [O III] line in A383-5.1. We extract the spectrum based on the 3σ level of the moment-0 map, and the peak is detected at 12σ. The spectrum and the moment-0 map are shown in Figure 1 (the moment-0 contours are overlaid on the NIRCam F200W image), and the resulting parameters of a single Gaussian line profile are $S_{\rm peak} = 7.9 \pm 1.1$ mJy, linewidth FWHM = 99 ± 15 km s^{-1}, which corresponds to an integrated line intensity of 0.83 ± 0.16 Jy km s^{-1}. The estimated redshift is $z = 6.0275 \pm 0.0002$, consistent with the [C II] redshift of $z = 6.0274 \pm 0.0002$. Similarly, the linewidth as given by FWHM is consistent with that derived for the [C II] line of 100 ± 23 km s^{-1} (Knudsen et al. 2016). Results are summarized in Table 1.

The estimated size given as the FWHM of the spatial distribution, based on a two-dimensional fit to the moment-0 map, is $(0.58 \pm 0.07)'' \times (0.22 \pm 0.07)''$ (PA = 20°), corresponding to an

Table 1. Observed and estimated properties from the [O III] line of A383-5.1

Parameter	Value
$z_{[OIII]}$	6.0275 ± 0.0002
S_{peak}	7.9 ± 1.1 mJy
FWHM	99 ± 15 km s^{-1}
$I_{[OIII]}$	0.83 ± 0.16 Jy km s^{-1}
$L_{[OIII]}$	$(1.29 \pm 0.24) \times 10^8$ L$_\odot$
SFR$_{[OIII]}$	5.6 M$_\odot$ yr^{-1}

Notes. The line luminosity and SFR are corrected for gravitational lensing magnification.

area of 0.1 arcsec^2. Correcting for gravitational lensing magnification, this corresponds to an area of 0.3 kpc^2. This is consistent with the *HST* WFC3/F110W continuum imaging results from Richard et al. (2011), who noted that the Lyman-α emission is more extended.

In Knudsen et al. (2016), the angular resolution of the [C II] detection was not sufficient to resolve the line emission. Combining with the archival data with similar depth but longer baselines[1], we find a similar result for the line profile. We note that the better *uv*-coverage shows also extended [C II]. A two-dimensional Gaussian fit yields $(0.38 \pm 0.09)'' \times (0.24 \pm 0.09)''$ (PA = 8.8°), consistent with the [O III] result. We note that the [C II] detection has a lower significance than the [O III] one, and therefore the accuracy of the size of the [C II] emission is lower.

We estimate the [O III] line luminosity using $L_{line} = 1.04 \times 10^{-3} S\Delta V D_L^2 \nu_{obs}$ (e.g. Solomon & Vanden Bout 2005; Carilli & Walter 2013) to be $L_{[OIII]} = (1.29 \pm 0.24) \times 10^8$ L$_\odot$ corrected for lensing magnification; the uncertainty reflects the propagated error from the Gaussian fit to the line profile. De Looze et al. (2014) have investigated the [O III] line as a SFR estimator for local star-forming galaxies against other probes, and for different classes of galaxies. Using the relation for low-metallicity galaxies we estimate SFR$_{[OIII]} \sim 5.6$ M$_\odot$ yr^{-1}, which is above other previous estimates for the SFR based on optical and [C II] results (Richard et al. 2011; Stark et al. 2015; Knudsen et al. 2016). The estimated [C II] line luminoity is $L_{[CII]} = (8.9 \pm 3.1) \times 10^6$ L$_\odot$ (Knudsen et al. 2016), which implies a line luminosity ratio of [O III]/[C II] $\sim 14 \pm 5$.

Continuum emission is undetected in the band-8, and we place a 3σ upper limit of 0.105 mJy. We use this together with the upper limit from the band-6 observations to estimate an upper limit of the far-infrared luminosity. Assuming a modified blackbody spectral energy distribution with a temperature $T = 35$ K and $\beta = 1.6$ (and correcting for the CMB radiation field), we find $L_{FIR} < 5.6 \times 10^9$ L$_\odot$. This is consistent with the upper limit based on the band-6 observations from Knudsen et al. (2016). For higher T, the upper limit on L_{FIR} will approach $< 10^{10}$ L$_\odot$. Similarly, if selecting a slightly higher β will similarly increase the upper limit; results from Faisst et al. (2020) suggests β values between 1.6 and 2.4 for high-z galaxies. Assuming the total IR luminosity to be about 30% higher (e.g. Decarli et al. 2017), and assuming a conversion SFR[M$_\odot$ yr^{-1}] $= 1.07 \times 10^{-10} L_{IR}$[L$_\odot$] (Calzetti 2013, assuming a Kroupa IMF in the mass range 0.1-100 M$_\odot$ and a timescale of constant star formation of $\tau = 100$ Myr), this would correspond to an SFR < 0.4 M$_\odot$ yr^{-1} (or < 0.8 M$_\odot$ yr^{-1} if using $T = 45$ K), which is below that of optical and [O III]-based estimates; keeping in mind a higher dust temperature would imply a higher upper limit on the L_{FIR} and thus also a higher upper limit on the SFR. This is implies that the obscured fraction of star formation is small.

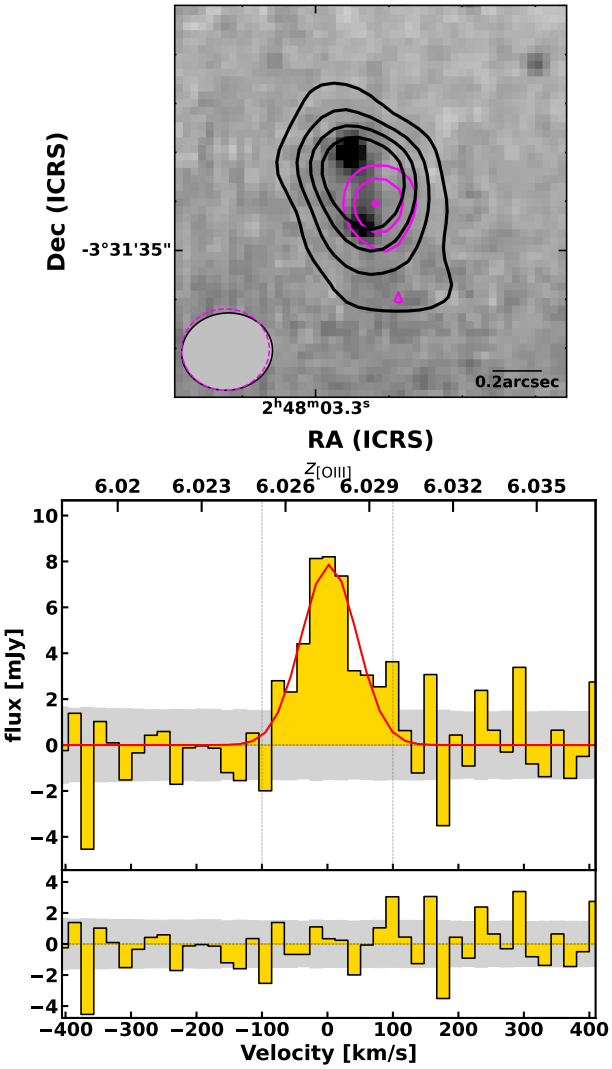

Fig. 1. The [O III] 88 μm detection of A383-5.1. *Top*: Moment-0 map obtained through collapsing the data cube over the velocity range -100 to 100 km/s. The contours show $3, 5, 7, 9\sigma$, and dashed show -3σ overlaid on the *JWST* NIRCam/F200W image. Additionally, the magenta contours show the moment-0 of [C II] using the combined data from Knudsen et al. (2016) and additional ALMA archive data; [C II] contours show $3, 4, 5\sigma$. *Bottom*: ALMA spectra extracted at the position of A383-5.1 and centered at the frequency of the redshifted [O III] line. The red dashed line shows the best-fit Gaussian. The vertical lines indicate the velocity range over which the moment-0 map has been extracted. The lower panel shows the residuals after subtracting the best-fit Gaussian profile from the spectrum.

With two continuum upper limits in band-6 and band-8 it is not possible to constrain the far-infrared SED shape. However, we can estimate an upper limit on the dust mass. We use the 3σ limit from the band-6 data of $f_{\nu_{obs}=270\,GHz} < 0.033$ mJy and the band-8 upper limit, and assume that the dust follows local galaxy properties with an absorption coefficient of $\kappa_{88\mu m} = 44.1$ cm^2 g^{-1} and $\kappa_{158\mu m} = 12.0$ cm^2 g^{-1} (e.g. Draine & Li 2007; Draine et al. 2014). For $S_{\nu_{obs}} \propto \kappa_{\nu_{rest}} B_{\nu_{rest}}(T) M_d$, where ν_{rest} is the rest-frame frequency and ν_{obs} is the redshifted frequency, we assume $T = 35$ K and estimate an upper limit on the dust mass $M_d < 0.8 \times 10^6$ M$_\odot$ (corrected for lensing magnification and the

[1] Project number: 2015.1.01136.S

effect of the CMB); a higher dust temperature would result in an even lower dust mass limit. Figs. 2 and 3 show the FIR upper limit on the continuum together with modified blackbody functions for a range of temperature and β, and the upper limit on the dust mass as function of temperature using the two upper limits. While each individual upper limit does not provide a solid upper limit, together they provide a marginally improved constraint if fixing the modified blackbody to one of the photometric upper limits. The dust mass upper limit is similar to the dust mass upper limits for sample of stacked gravitationally lensed $z \sim 6$ galaxies (Jolly et al. 2021). Without knowledge of dust properties and dust temperature, this estimate remains uncertain, nonetheless it shows that A383-5.1 is a dust-poor system. This deep upper limit on the dust mass results in valuable constraints on the nature of A383-5.1. If the rest-frame optical emission of this source is from a star-forming galaxy, the galaxy mass is estimated around $\log_{10} M_\star/\mathrm{M}_\odot = 8.9$, while the presence of an optically-luminous AGN would reduce this stellar mass to $\log_{10} M_\star/\mathrm{M}_\odot = 7.7$ (Golubchik et al. 2025). Assuming a dust temperature of around 40 K, the subsequent dust-to-stellar mass ratios in these two scenarios vary between an extremely dust-poor ($< 3 \times 10^{-4}$) galaxy, and a low dust presence of ($< 7 \times 10^{-3}$) in the interstellar medium surrounding an AGN system.

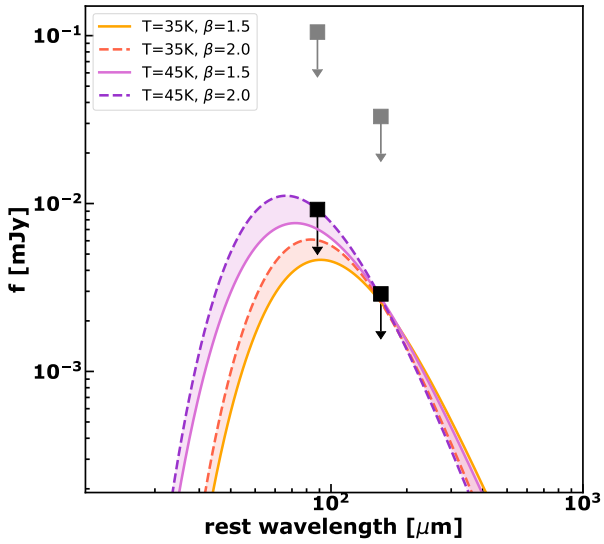

Fig. 2. The far-IR SED of A383-5.1 with the two continuum upper limits from bands 6 and 8. The grey squares show the 3σ observed limits, while the black squares show the same corrected for gravitational lensing magnification. The modified blackbody functions are normalised to the band-6 data point.

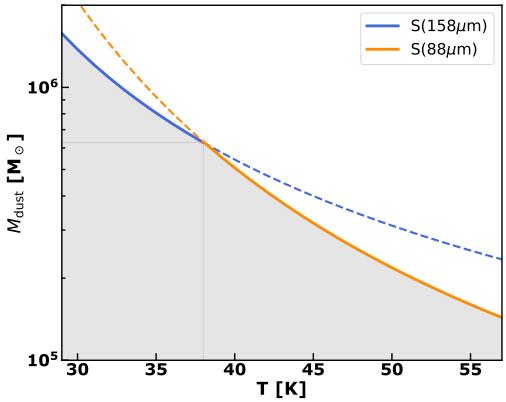

Fig. 3. Estimate on the 3σ upper limit of the dust mass as a function of temperature T and with the assumed k_ν values given in the text. The blue [orange] line shows the limit when normalising to the band-6 [band-8] upper limits. When normalising to one of the upper limits, it places a constraint on the temperature, which is indicated with the dashed line. The grey area indicates the range of dust masses as a function of the dust temperature between $T = 30 - 55$ K. Along this range, the mass limit changes by more than a factor 8.

4. Discussion

The very high magnification factor of A383-5.1 has allowed for the first ALMA detection of far-infrared fine structure emission lines to be detected in a low stellar mass galaxy hosting an LRD[2]. The observed high line ratio combined with the LRD identification suggests that this galaxy is not akin to local analogs (e.g., low-metallicity dwarf galaxies, e.g., Cormier et al. 2015), but is rather part of the new extreme population revealed by *JWST*. Therefore, we begin by discussing the high line ratio in this context.

The [O III] detection, and the previous [C II] detection, are the first far-infrared fine-structure line detections in an LRD. Focusing first on how the line properties relate to star formation measurements, we compare to local galaxies, where a relation is seen between SFR and far-infrared fine-structures lines [C II] 158μm, [O III] 88μm, and [O I] 63μm (e.g. De Looze et al. 2014). In the case of the [O III] line, there appears to be up to an order of magnitude difference in the estimated SFR-line luminosity relation depending on properties such as the metallicity. Based on an analysis prior to *JWST* observations, the second lensed image, A383-5.2, has an estimated metallicity of $Z \sim (0.043^{+0.030}_{-0.013})Z_\odot$ and mass of $\sim 3 \times 10^9\,\mathrm{M}_\odot$ (Richard et al. 2011; Stark et al. 2015), indicating that the system could be similar to local low-Z dwarf galaxies. Low-metallicity dwarf galaxies have a significantly higher average [O III] line luminosity than starbursts for similar SFR. Assuming the estimated SFR of $2.0^{+0.34}_{-0.3}\,\mathrm{M}_\odot\,\mathrm{yr}^{-1}$ (Richard et al. 2011; Stark et al. 2015), A383-5.1 follows this trend within the scatter of the local relation for low-Z dwarf galaxies. In Fig. 4, we plot the $L_{[\mathrm{OIII}]}$ vs. SFR together with other $z > 6$ [O III] detections. But contrasting this with the discussion of the SFR based on the new *JWST*/NIRCam results, which suggests that the SFR cannot exceed $0.5\,\mathrm{M}_\odot\,\mathrm{yr}^{-1}$ (Golubchik et al. 2025), this would indicate that the [O III] is to a large extend not powered by star formation, but rather by some other mechanism (e.g., by ionization from the radiation field from a growing super-massive black hole); the location of the NIRCam-estimated SFR is also indicated in Fig. 4 and shows how the [O III] line luminosity exceeds the local relation between SFR and $L_{[\mathrm{OIII}]}$.

The specific SFR, sSFR = SFR/M_{stellar}, is $\sim 10^{-8}\,\mathrm{yr}^{-1}$ assuming the values including the BH* interpretation of the LRD Golubchik et al. (2025); the sSFR would be lower, though assuming a model without BH*. As discussed in Algera et al. (2024b, 2025), a high [O III]/[C II] ratio could be indicative of a system of high burstiness. The sSFR together with the line ratio could suggest that components of A383-5.1 is a young system, which would be in agreement with the SED modelling results for the blue companion (Golubchik et al. 2025; Baggen et al. 2025). We note the large uncertainties in the sSFR, though, making it challenging to make conclusive statements on this.

[2] Xiao et al. (2025) did targetted ALMA observations of two massive and bright LRDs and placed upper limits on the [C II] line luminosity and thermal dust luminosity.

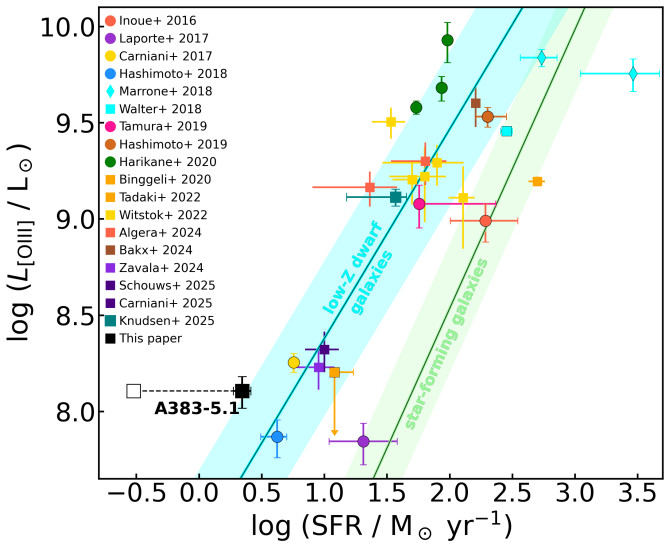

Fig. 4. [O III] line luminosity, $L_{[OIII]}$, vs. star formation rate. The filled black square shows the detection in A383-5.1 using the SFR of Richard et al. (2011), and the open black square shows the same but with the SFR limit of Golubchik et al. (2025), while the coloured symbols show recent results (Inoue et al. 2016; Carniani et al. 2017; Laporte et al. 2017; Marrone et al. 2018; Hashimoto et al. 2018; Tamura et al. 2019; Hashimoto et al. 2019; Harikane et al. 2020; Binggeli et al. 2021; Akins et al. 2022; Algera et al. 2024a; Tadaki et al. 2022; Witstok et al. 2022; Bakx et al. 2024; Zavala et al. 2024; Schouws et al. 2025; Carniani et al. 2025; Knudsen et al. 2025). The $L_{[OIII]}$ - SFR relation, where The green region shows the $L_{[OIII]}$ - SFR relation for local star-forming galaxies, and the light-blue one shows that for low-metallicity dwarf galaxies (De Looze et al. 2014).

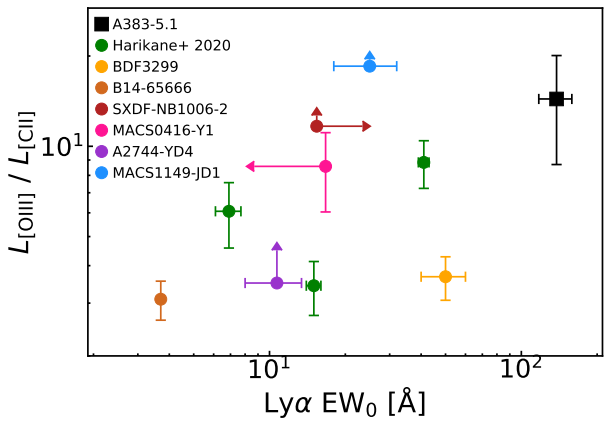

Fig. 5. The [O III] / [C II] line luminosity ratio vs. the Lyα equivalent width. Black square shows the detection in A383-5.1, and coloured symbols show results for other $z > 6$ galaxies (Vanzella et al. 2011; Shibuya et al. 2012; Furusawa et al. 2016; Inoue et al. 2016; Carniani et al. 2017; Laporte et al. 2017, 2019; Hashimoto et al. 2018; Tamura et al. 2019; Hashimoto et al. 2019; Harikane et al. 2020).

The new *JWST*/NIRCam imaging shows that A383-5.1 resolves into two sources, a red compact source hosting an LRD, and a blue companion source (Golubchik et al. 2025), with a possible indication of bridging emission between the components (Baggen et al. 2025). The distribution of the [O III] emission relative to the *JWST*/NIRCam imaging is shown in Fig. 1. Generally the distribution of the [O III] emission follows that of the overall structure of the entire system from the *JWST* imaging, although we note the angular resolution of the ALMA observations is lower than that of the NIRCam F200W image. The [C II] observations, which have a lower signal-to-noise ratio, are similarly limited by the angular resolution, but appear to be centered between the blue and red component (Golubchik et al. 2025). Due to the limited angular resolution and signal-to-noise ratio, we cannot currently constrain if only a single component in the system is responsible for the majority of one or both of the far-infrared emission lines, and therefore not determine if the emission is powered by star formation or a rapidly growing supermassive black hole.

The population of LRDs has been found to be dust poor (Casey et al. 2025), which is also the case for A383-5.1 with no dust emission detection in both ALMA band 6 and 8 observations (corresponding to the [C II] and [O III] measurements). The observed low dust content in A383-5.1 implies a low dust attenuation of the UV radiation. This is consistent with the bright [O III] line observations, as photons with energy > 35 eV are required to double ionize oxygen. Generally, the possible impact of dust obscuration seem negligible, which is consistent with the estimated low metallicity in the system (Richard et al. 2011; Stark et al. 2015; Golubchik et al. 2025).

With a redshift of z = 6.027, A383-5.1 is near the end of the EoR (e.g., Planck Collaboration et al. 2016), and given the large Lyα equivalent width, it is likely not located in a neutral region of the intergalactic medium (IGM). As pointed out by, e.g., Harikane et al. (2020), there appears to be a trend of increasing [O III]/[C II] line luminosity ratio with increasing Lyα equivalent width (EW) as seen for $z > 6$ Lyman Break Galaxies. This trend can be interpreted as these high-z galaxies having high ionization parameters and/or low PDR covering factors, meaning that there is a deficiency of neutral gas surrounding H II regions (Harikane et al. 2020). With the high line luminosity ratio and large Lyα EW $\sim$ 140 Å (Stark et al. 2015) A383-5.1 follows this trend; in Fig. 5, we plot the [O III]/[C II] line luminosity ratio as function of Lyα EW for comparison with other results. This suggests that the neutral gas content of sub-L* galaxies like A383-5.1 may be even lower, which would lead to a higher escape fraction of ionizing UV photons. If correct, this would naturally lend support to the suggestion that sub-L* star-forming galaxies make a significant (and likely a dominant) contribution to the EoR (e.g., McLure et al. 2013; Bouwens et al. 2016; Parsa et al. 2018; Ishigaki et al. 2018). Even though A383-5.1 is observed near the end of the EoR, the properties of A383-5.1 could be similar to those of sub-L* galaxies 100-200 million years earlier, thus providing insights to the EoR sub-L* population. Given its low metallicity, dust content, and high degree of ionization, the Lyman continuum escape fraction is likely significant.

Gravitational lensing is key to explore populations of fainter galaxies, with lower stellar masses and star-formation rates. Our source, as well as the z = 9.1 MACS1149-JD1 (Hashimoto et al. 2018), allow us to characterize the sub-L* population, best representative of the evolution of the bulk of galaxies across cosmic time. Even with magnification factors of $\mu > 9$, both sources required $\sim$ 10 hr on-source time for detection with ALMA. In order to expand samples of these more lower-luminosity galaxies during the EoR, extensive observing time needs to be involved. ALMA, and its future updates including the Wideband Sensitivity Upgrade (Carpenter et al. 2023), will play an immense role in developing our understanding of the nature of the numerous, but lower luminosity galaxies in the EoR.

5. Summary

We report the detection of the [O III] 88μm emission line from the $z = 6.027$ star-forming galaxy A383-5.1, which based on recent *JWST* observations has been identified to include an LRD. The combination of an 8-hours on-source integration with a gravitational lensing magnification of $\mu = 11.4 \pm 1.9$, makes these data among the deepest band-8 images of a $z \sim 6$ source so far. [O III] is detected at 12σ with an integrated line intensity of $0.83 \pm 0.16\,\mathrm{Jy\,km\,s^{-1}}$ (the error reflects the uncertainty from the Gaussian fit to the line profile) and a line luminosity of $L_{[\mathrm{OIII}]} = (1.29 \pm 0.24) \times 10^8\,\mathrm{L_\odot}$. The redshift and line width are consistent with that of our previous [C II] detection. The emission is resolved over an area of $0.3\,\mathrm{kpc^2}$ (corrected for lensing magnification). The continuum non-detection is consistent with the previous band-6 non-detection, and we estimate an upper limit on the dust mass of $0.8 \times 10^6\,\mathrm{M_\odot}$, assuming dust properties similar to Galactic dust, and note that for other assumptions, e.g., higher dust temperature, the upper limit would be even lower and close to $10^5\,\mathrm{M_\odot}$. Compared to its stellar mass, this is very low, and thus indicates that the galaxy is extremely dust-poor. The derived [O III] to [C II] luminosity ratio is ~ 14, which is large compared to normal star-forming galaxies, but consistent with low-metallicity, low-stellar mass galaxies in the local universe.

The recent *JWST*/NIRCam discovery of this system containing two components, an LRD and a blue companion, would imply that A383-5.1 is among the few LRDs with successful far-infrared emission line detections. The high [O III]/[C II] line ratio, a possible sign of a strong UV radiation field, could be provide a means for finding embedded growing black holes, if this is indeed the nature of LRDs. The relatively bright [O III] detection together with the high [O III]/[C II] line ratio also could imply that the system is experiencing a burst-like episode, especially considering the fact that there are two components and possibly a bridge of emission between the two.

A383-5.1 is a sub-L* galaxy, and therefore in the luminosity range of galaxies that have been proposed to contribute significantly to the ultraviolet emission that reionizes the IGM during the epoch of reionization. With the remarkably low dust-mass and high [O III]/[C II] line ratio, dust attenuation will not significantly impact the escape fraction of ionizing UV-photons. Our results demonstrate the need for high-frequency ALMA observations for detailed studies of the lower luminosity galaxy population that likely could be responsible for a significant fraction of the reionization.

Acknowledgements. We acknowledges support from the Nordic ALMA Regional Centre (ARC) node based at Onsala Space Observatory. The Nordic ARC node is funded through Swedish Research Council grant No 2017-00648. KKn and KKa acknowledge support from the Knut and Alice Wallenberg Foundation (KAW 2017.0292). KKn and RR acknowledge support from the ERC synergy grant 101166930 (RECAP). MJ is supported by the United Kingdom Research and Innovation (UKRI) Future Leaders Fellowship 'Using Cosmic Beasts to uncover the Nature of Dark Matter' (grant numbers MR/S017216/1 & MR/X006069/1). This project was also supported by the Science and Technology Facilities Council [grant number ST/L00075X/1]. This paper makes use of the following ALMA data: ADS/JAO.ALMA#2016.1.00333.S, 2015.1.01136.S, and 2013.1.01241.S. ALMA is a partnership of ESO (representing its member states), NSF (USA) and NINS (Japan), together with NRC (Canada) and NSC and ASIAA (Taiwan) and KASI (Republic of Korea), in cooperation with the Republic of Chile. The Joint ALMA Observatory is operated by ESO, AUI/NRAO and NAOJ.

References

Akins, H. B., Fujimoto, S., Finlator, K., et al. 2022, ApJ, 934, 64
Algera, H., Rowland, L., Smit, R., et al. 2025, arXiv e-prints, arXiv:2509.16071
Algera, H. S. B., Inami, H., Sommovigo, L., et al. 2024a, MNRAS, 527, 6867
Algera, H. S. B., Inami, H., Sommovigo, L., et al. 2024b, MNRAS, 527, 6867
Baggen, J. F. W., van Dokkum, P., Labbé, I., & Brammer, G. 2025, arXiv e-prints, arXiv:2512.03239
Bakx, T. J. L. C., Algera, H. S. B., Venemans, B., et al. 2024, MNRAS, 532, 2270
Binggeli, C., Inoue, A. K., Hashimoto, T., et al. 2021, A&A, 646, A26
Bouwens, R. J., Oesch, P. A., Labbé, I., et al. 2016, ApJ, 830, 67
Bouwens, R. J., Smit, R., Schouws, S., et al. 2022, ApJ, 931, 160
Bradač, M., Garcia-Appadoo, D., Huang, K.-H., et al. 2017, ApJ, 836, L2
Calzetti, D. 2013, in Secular Evolution of Galaxies, ed. J. Falcón-Barroso & J. H. Knapen, 419
Carilli, C. L. & Walter, F. 2013, ARA&A, 51, 105
Carniani, S., D'Eugenio, F., Ji, X., et al. 2025, A&A, 696, A87
Carniani, S., Maiolino, R., Pallottini, A., et al. 2017, A&A, 605, A42
Carpenter, J., Brogan, C., Iono, D., & Mroczkowski, T. 2023, in Physics and Chemistry of Star Formation: The Dynamical ISM Across Time and Spatial Scales, ed. V. Ossenkopf-Okada, R. Schaaf, I. Breloy, & J. Stutzki, 304
Casey, C. M., Akins, H. B., Finkelstein, S. L., et al. 2025, ApJ, 990, L61
Cormier, D., Madden, S. C., Lebouteiller, V., et al. 2015, A&A, 578, A53
De Looze, I., Cormier, D., Lebouteiller, V., et al. 2014, A&A, 568, A62
Decarli, R., Walter, F., Venemans, B. P., et al. 2017, Nature, 545, 457
Draine, B. T., Aniano, G., Krause, O., et al. 2014, ApJ, 780, 172
Draine, B. T. & Li, A. 2007, ApJ, 657, 810
Faisst, A. L., Fudamoto, Y., Oesch, P. A., et al. 2020, MNRAS, 498, 4192
Finkelstein, S. L., Papovich, C., Dickinson, M., et al. 2013, Nature, 502, 524
Fontanot, F., Cristiani, S., & Vanzella, E. 2012, MNRAS, 425, 1413
Fudamoto, Y., Smit, R., Bowler, R. A. A., et al. 2022, ApJ, 934, 144
Fujimoto, S., Kohno, K., Ouchi, M., et al. 2024, ApJS, 275, 36
Fujimoto, S., Oguri, M., Brammer, G., et al. 2021, ApJ, 911, 99
Furusawa, H., Kashikawa, N., Kobayashi, M. A. R., et al. 2016, ApJ, 822, 46
Golubchik, M., Furtak, L. J., Allingham, J. F. V., et al. 2025, arXiv e-prints, arXiv:2512.02117
Greene, J. E., Labbe, I., Goulding, A. D., et al. 2024, ApJ, 964, 39
Grissom, R. L., Ballantyne, D. R., & Wise, J. H. 2014, A&A, 561, A90
Harikane, Y., Ouchi, M., Inoue, A. K., et al. 2020, ApJ, 896, 93
Hashimoto, T., Inoue, A. K., Mawatari, K., et al. 2019, PASJ, 71, 71
Hashimoto, T., Laporte, N., Mawatari, K., et al. 2018, Nature, 557, 392
Hassan, S., Davé, R., Mitra, S., et al. 2018, MNRAS, 473, 227
Inami, H., Algera, H. S. B., Schouws, S., et al. 2022, MNRAS, 515, 3126
Inoue, A. K., Tamura, Y., Matsuo, H., et al. 2016, Science, 352, 1559
Ishigaki, M., Kawamata, R., Ouchi, M., et al. 2018, ApJ, 854, 73
Jolly, J.-B., Knudsen, K., Laporte, N., et al. 2021, A&A, 652, A128
Knudsen, K. K., Richard, J., Kneib, J.-P., et al. 2016, MNRAS, 462, L6
Knudsen, K. K., Watson, D., Richard, J., et al. 2025, A&A, 701, A85
Kocevski, D. D., Onoue, M., Inayoshi, K., et al. 2023, ApJ, 954, L4
Labbé, I., Greene, J. E., Bezanson, R., et al. 2025, ApJ, 978, 92
Labbé, I., van Dokkum, P., Nelson, E., et al. 2023, Nature, 616, 266
Laporte, N., Ellis, R. S., Boone, F., et al. 2017, ApJ, 837, L21
Laporte, N., Katz, H., Ellis, R. S., et al. 2019, MNRAS, 487, L81
Laporte, N., Zitrin, A., Ellis, R. S., et al. 2021, MNRAS, 505, 4838
Madau, P. & Dickinson, M. 2014, ARA&A, 52, 415
Maiolino, R., Carniani, S., Fontana, A., et al. 2015, MNRAS, 452, 54
Maiolino, R., Risaliti, G., Signorini, M., et al. 2025, MNRAS, 538, 1921
Marrone, D. P., Spilker, J. S., Hayward, C. C., et al. 2018, Nature, 553, 51
McLure, R. J., Dunlop, J. S., Bowler, R. A. A., et al. 2013, MNRAS, 432, 2696
McMullin, J. P., Waters, B., Schiebel, D., Young, W., & Golap, K. 2007, in Astronomical Society of the Pacific Conference Series, Vol. 376, Astronomical Data Analysis Software and Systems XVI, ed. R. A. Shaw, F. Hill, & D. J. Bell, 127
Naidu, R. P., Matthee, J., Katz, H., et al. 2025, arXiv e-prints, arXiv:2503.16596
Oesch, P. A., van Dokkum, P. G., Illingworth, G. D., et al. 2015, ApJ, 804, L30
Ota, K., Walter, F., Ohta, K., et al. 2014, ApJ, 792, 34
Ouchi, M., Ellis, R., Ono, Y., et al. 2013, ApJ, 778, 102
Parsa, S., Dunlop, J. S., & McLure, R. J. 2018, MNRAS, 474, 2904
Perger, K., Fogasy, J., Frey, S., & Gabányi, K. É. 2025, A&A, 693, L2
Planck Collaboration, Adam, R., Aghanim, N., et al. 2016, A&A, 596, A108
Planck Collaboration, Aghanim, N., Akrami, Y., et al. 2020, A&A, 641, A6
Remijan, A., Biggs, A., Cortes, P. A., et al. 2019, ALMA Technical Handbook,ALMA Doc. 7.3, ver. 1.1, 2019, ALMA Technical Handbook,ALMA Doc. 7.3, ver. 1.1ISBN 978-3-923524-66-2
Richard, J., Kneib, J.-P., Ebeling, H., et al. 2011, MNRAS, 414, L31
Schenker, M. A., Stark, D. P., Ellis, R. S., et al. 2012, ApJ, 744, 179
Schouws, S., Bouwens, R. J., Ormerod, K., et al. 2025, ApJ, 988, 19
Sekimoto, Y., Iizuko, Y., Satou, N., et al. 2008, in Ninteenth International Symposium on Space Terahertz Technology, ed. W. Wild, 253–257
Shibuya, T., Kashikawa, N., Ota, K., et al. 2012, ApJ, 752, 114
Solomon, P. M. & Vanden Bout, P. A. 2005, ARA&A, 43, 677
Sommovigo, L., Ferrara, A., Pallottini, A., et al. 2022, MNRAS, 513, 3122
Stark, D. P. 2016, ARA&A, 54, 761
Stark, D. P., Richard, J., Charlot, S., et al. 2015, MNRAS, 450, 1846
Tadaki, K.-i., Tsujita, A., Tamura, Y., et al. 2022, PASJ, 74, L9
Tamura, Y., Mawatari, K., Hashimoto, T., et al. 2019, ApJ, 874, 27
Vanzella, E., Pentericci, L., Fontana, A., et al. 2011, ApJ, 730, L35
Watson, D., Christensen, L., Knudsen, K. K., et al. 2015, Nature, 519, 327
Witstok, J., Smit, R., Maiolino, R., et al. 2022, MNRAS, 515, 1751
Xiao, M., Oesch, P. A., Bing, L., et al. 2025, A&A, 700, A231
Zavala, J. A., Bakx, T., Mitsuhashi, I., et al. 2024, ApJ, 977, L9
Zitrin, A., Labbé, I., Belli, S., et al. 2015, ApJ, 810, L12